ELSEVIER

International Journal of Mass Spectrometry 185/186/187 (1999) 61–73

International Journal of Mass Spectrometry

Mass spectrometric study of unimolecular decompositions of endohedral fullerenes

J. Laskin[a], T. Peres[a], A. Khong[b], H.A. Jiménez-Vázquez[b], R.J. Cross[b], M. Saunders[b], D.S. Bethune[c], M.S. de Vries[a], C. Lifshitz[a,*]

[a]*Department of Physical Chemistry and The Farkas Center for Light Induced Processes, The Hebrew University of Jerusalem, Jerusalem 91904, Israel*

[b]*Chemistry Department, Yale University, Box 208107, New Haven, CT 06520-8107, USA*

[c]*Almaden Research Center, IBM Research Division, 650 Harry Road, San Jose, CA 95120, USA*

Received 22 April 1998; accepted 2 June 1998

Abstract

Unimolecular decompositions of noble gas containing endohedral fullerenes as well as metallofullerenes were studied using tandem mass spectrometry techniques. Endohedral fullerenes do not lose the endohedral atom unimolecularly but fragment via the loss of C_2 units. Kinetic energy release distributions were measured for the emission of C_2 units from the positive ions of C_{60}, Ne@C_{60}, Ar@C_{60}, Kr@C_{60}, C_{82}, La@C_{82}, Tb@C_{82}, C_{84}, and Sc_2@C_{84}. These distributions were analyzed using both a model free approach, and a formalism developed by Klots, based on decomposition in a spherically symmetric potential. The C_2 binding energies were deduced from the models. Noble gas atoms are shown to stabilize the fullerene cage. The C_2 binding energies increase in the order: $\Delta E_{vap}(C_{60}^+) < \Delta E_{vap}(Ne@C_{60}^+) < \Delta E_{vap}(Ar@C_{60}^+) < \Delta E_{vap}(Kr@C_{60}^+)$. Endohedral metal atoms have a strong effect on the cage binding. The C_2 binding energy in La@C_{82}^+ is about 1.5 eV higher than that in C_{82}^+. The Tb atom has an even stronger effect with a binding energy of about 3 eV higher than for C_{82}^+. The emission of a C_2 unit from the dimetallofullerenes Sc_2@C_{84}^+ and Tb_2@C_{84}^+ was studied as well. Two Sc atoms have a slight destabilizing effect on C_{84}, whereas two Tb atoms stabilize the cage. (Int J Mass Spectrom 185/186/187 (1999) 61–73) © 1999 Elsevier Science B.V.

Keywords: Binding energies; Endohedral fullerenes; KERDs (kinetic energy release distributions)

1. Introduction

One of the fascinating properties of fullerenes is their ability to trap atoms and small molecules inside the cage. The first evidence for endohedral metallofullerenes was reported soon after the discovery of C_{60} in 1985 [1]. However, only in 1991 could endohedral metallofullerenes be isolated in macroscopic amounts. This was achieved by using laser or arc vaporization [2] of graphite-metal composites in helium. Numerous metallofullerenes containing most of the lanthanide elements have been synthesized using these methods. Extended x-ray absorption fine structure (EXAFS) experimental results [3] were consistent with the hypothesis that yttrium metal atoms are trapped inside the fullerene cage. Ion mobility studies of LaC_n^+ [4] demonstrated that the species with n = 38–90 were endohedral. The endohedral nature of the

* Corresponding author.

Dedicated to Professor Michael T. Bowers, one of the pioneers in this field of research, on the occasion of his 60th birthday.

PII S1387-3806(98)14060-5

yttrium compound, $Y@C_{82}$ has recently been confirmed unequivocally using x-ray diffraction [5]. It has been shown that the metal atom is indeed inside the fullerene cage and is strongly bound to the cage.

The experimental procedure for isolation and separation of endohedral metallofullerenes is well developed now; however a detailed investigation of the properties of these molecules is still difficult due to the low yields of production. Electronic and geometric structures of different mono- and dimetallofullerenes have been extensively studied experimentally and theoretically in recent years [2b,6]. It has been shown that endohedral metal atoms donate two or three valence electrons to the carbon cage [7,8] depending on their properties and, therefore, form strong bonding with the cage. Structures of many dimetallofullerenes have been determined both experimentally (using NMR) and theoretically as summarized in a recent review [9], whereas the structures for most of the monometallofullerenes could not be determined using the NMR technique due to their paramagnetic nature. Collisional [10] and photoionization [11] fragmentation patterns of $La@C_{82}$ have been measured. The fullerene cage shrinks by successive C_2 losses, just like empty fullerenes. Ejection of a metal atom with one or more C_2 units upon collisions has been demonstrated as well. Little is known about the energetics and dynamics of metallofullerene ion evaporations. Recently, we compared the kinetic energy releases upon dissociation of $La@C_{82}^+$ and empty C_{82}^+ [12]. We found that the C_2 binding energy in $La@C_{82}^+$ is about 1 eV higher than that in C_{82}^+.

Endohedral fullerenes with a noble gas atom inside the fullerene cage were first observed by Schwarz and co-workers in high-energy ion beam collision experiments [13,14]. Saunders and co-workers have shown that neutral noble gas compounds can be prepared by heating fullerenes under high pressure of a noble gas [15,16]. Endohedral fullerenes of all the noble gases were prepared using this method. Typical yields of incorporation are around 0.2% for helium, neon, argon, and krypton and around 0.04% for xenon. In order to explain incorporation of noble gas atoms inside fullerenes, as well as their release, a mechanism was proposed involving reversibly breaking a bond to open a "window" in the cage, thus allowing easy incorporation of guest atoms. It has been shown that the barrier for the release of helium from $He@C_{60}$ under thermal conditions is about 3.5 eV [15]. The more recently accepted value for the C_2 binding energy of C_{60}^+ is 7.1 eV [17] implying that $He@C_{60}^+$ should easily lose its He atom. However, according to high-energy collision experiments [13], $He@C_{60}^+$ does not undergo the He release reaction but rather dissociates via the elimination of C_2 units. Campbell and co-workers [18] determined the barrier for He capture and release in collision experiments and showed that it was dependent on the internal energy of the fullerene projectile ion with a lower limit of about 6–8 eV. A radical impurity ("promoter") mechanism provided a different mechanistic interpretation of the high-pressure experiments [19]. As a result of more recent data [19b] it became clear that the originally suggested barrier of 3.5 eV [15] for the release of He from C_{60} is probably incorrect. Apparently, traces of solvent left in the crystal initiate a radical chain reaction that destroys the fullerene. Unimolecular fragmentation of $Ne@C_{60}^+$ was recently studied by us [12]. It has been shown that a Ne endohedral atom has a minor effect on the stability of the cage. The C_2 binding energy in $Ne@C_{60}^+$ is slightly higher than that in C_{60}^+. Collisional fragmentation of ionic $Ar@C_{60}$ has been studied [20,21]. Ejection of the Ar atom was observed in some cases in addition to C_2 evaporation, particularly in the case of negative ions. Recently, fragmentation of $M@C_{60}^+$ (M = He, Ne, Ar, Kr) upon collision with He was studied by Giblin et al. [22]. Endohedral fullerene fragments, empty fullerenes, and He containing complexes were found in the mass spectrum. The largest empty fragment was C_{60}^+ for $He@C_{60}^+$, C_{56}^+ for $Ne@C_{60}^+$, and C_{54}^+ for $Ar@C_{60}^+$ and $Kr@C_{60}^+$.

The determination of kinetic energy releases (KERs) upon unimolecular fragmentation provides valuable information on the energetics and dynamics of the reactions. Professor Bowers and his group have pioneered this kind of research in connection with carbon ion clusters, fullerenes, and organometallic compounds [23]. The C_2 binding energy of fullerenes and endohedral fullerenes can be determined through

modeling of experimental kinetic energy release distributions (KERDs). We present here a study of unimolecular fragmentations of some noble gas containing fullerenes, as well as mono- and dimetallofullerenes.

2. Experimental

Measurements were performed on a high-resolution double-focusing mass spectrometer of reversed geometry, the VG-ZAB-2F [24,25] using the technique of mass-analyzed ion kinetic energy (MIKE) spectrometry. The endohedral fullerene cations were obtained by ionization of the corresponding neutral samples, which were prepared by the methods described previously [2b,15].

The samples were introduced into the mass spectrometer using the direct insertion probe and evaporated at 400 °C. The electron-impact conditions were as follows: electron ionizing energy, 70 eV; emission current, 5 mA; ion source temperature, 400 °C; resolution, 1100 (10% valley definition). Metastable ion peak shapes were determined by scanning the electrostatic analyzer and using single-ion counting. Ion counting was achieved by a combination of an electron multiplier, amplifier/discriminator, and multichannel analyzer [26]. The experiments were performed at 8 kV acceleration voltage and a main beam width of 3–5 V. The data were accumulated in a computer controlled experiment, monitoring the main beam scan and correcting for the drift of the main beam [25]. The metastable ion peak shapes were mean values of 100–1000 accumulated scans. The product KERDs were determined from the first derivatives of the metastable ion peak shapes [27–29].

3. Data analysis

3.1. General background

The analysis of the experimental kinetic energy release distributions may be performed using two different approaches developed by Klots, namely, a model free approach [30] and a more generalized model which treats the unimolecular decomposition in a spherically symmetric potential (SSP) [31].

In the model free approach the KERD is written in the form [30]:

$$p(\epsilon) = \epsilon^l \exp(-\epsilon/k_B T^{\ddagger}) \qquad (0 < l < 1) \tag{1}$$

where ϵ is the kinetic energy release, l is a parameter that ranges from zero to unity depending on the interaction potential between the fragments, k_B is Boltzmann's constant, and $T^{\ddagger}$ is the transition state temperature defined by the average kinetic energy on passing through the transition state. The values of l and $T^{\ddagger}$ are obtained by fitting the experimental KERD with Eq. (1). The value of l which we found to give the best fit for all the KERDs (see below) is $l = 0.5$ (or slightly higher). This corresponds to the expected value for the most statistical situation, since the translational density of states is proportional to $\epsilon^{0.5}$ [32]. The isokinetic bath temperature defined as the temperature at which a heat bath should be set so that the canonical rate constant, $k(T_b)$, is equal to the microcanonical rate constant, $k(E)$, sampled in the experiment, is given by [30,33]:

$$T_b = T^{\ddagger} \frac{\exp(\gamma/C) - 1}{\gamma/C} \tag{2}$$

where γ is the Gspann parameter and C is the heat capacity in units of k_B minus one. Finally, the isokinetic bath temperature is related to the binding energy via the Trouton relation:

$$\Delta E_a = \gamma k_B T_b \tag{3}$$

The second approach (SSP) implies that the interaction of the separating fragments is described by a spherically symmetric potential. The KERD is given by:

$$[p(\epsilon) \propto \exp(-\epsilon/k_B T^{\ddagger})][1 - \exp(-BL_{\max}^2/k_B T^{\ddagger}] \tag{4}$$

where B is the rotational constant:

$$B = \frac{\hbar^2}{2(I_1 + I_2)}$$

I_1 and I_2 are the moments of inertia of the fragments, L_{max} is the maximum value of the orbiting angular momentum quantum number. L_{max} is obtained for known interaction potentials in the standard way. The derivation of L_{max} for some tractable potentials was discussed recently by Klots [34].

Both of the models described here have been applied to the experimental KERDs for reaction [30b,31a]:

$$C_{60}^+ \rightarrow C_{58}^+ + C_2 \quad (5)$$

It has been shown that the SSP model yields lower values for the binding energies compared to the model free approach [33]. The interaction potential used in [31] was of the form:

$$V(r) = \begin{cases} -\xi_4/r^4, & r > b \\ -\infty, & r < b \end{cases} \quad (6)$$

where b is the hard-sphere collision radius and ξ_4 the Langevin parameter.

A more realistic potential takes into account that a dissociating molecule is not a point charge but rather a sphere of diameter R_0 (this potential is applicable to fullerenes due to their cage structure) and is given by

$$V(r) = -e^2(k-1)R_0^3/[2(k+2)r^2(r^2-R_0^2)] \quad (7)$$

where k is the dielectric constant, e is the electron charge, and

$$(\hbar L)^2_{max} = 2\mu[(2\alpha e^2\epsilon)^{1/2} + \epsilon R_0^2] \quad (8)$$

where $\alpha = (k-1)R_0^3/(k+2)$ and μ is the reduced mass. Furthermore, a Gorin term ξ_6/r^6 may be introduced as a perturbation as discussed in [34]. The coefficient ξ_6 is given by

$$\xi_6 = \frac{3}{2}\alpha_1\alpha_2\frac{IE_1 IE_2}{IE_1 + IE_2} \quad (9)$$

where α_1, α_2 and IE_1, IE_2 are polarizabilities and ionization energies of the fragments.

3.2. Treating C_{60}^+

We have applied these models to the experimental KERD for reaction (5). C_{58}^+ was treated as a spherical shell implying that the moment of inertia is given by: $I_1 = 2/3MR^2$. The input parameters for the SSP calculations were as follows (most of the parameters were adopted from [33]): (1) Radius of C_{58}^+, $R = 3.2 \times 10^{-8}$ cm; (2) moment of inertia of C_{58}^+, $I_1 = 7.89 \times 10^{-37}$ g cm^2; (3) moment of inertia of C_2, $I_2 = 1.54 \times 10^{-39}$ g cm^2; (4) impact parameter between product fragments $b = 3.82 \times 10^{-8}$ cm; (5) polarizability of C_2, $\alpha_2 = 1.43 \times 10^{-24}$ cm^3; (6) polarizability of C_{58}^+, $\alpha_1 = 8.4 \times 10^{-23}$ cm^3 (assumed to be equal to the polarizability of C_{60} adopted from [35]); (7) C_{58} ionization energy $IE_1 = 7.07$ eV [36]; (8) C_2 ionization energy, $IE_2 = 12.11$ eV; (9) Gorin's parameter, $\xi_6 = 1.29 \times 10^{-57}$ erg cm^6. This value is two times higher than the value suggested by Klots [34]. The discrepancy is due to the difference in the polarizability of C_{58}^+; (10) Gspann parameter, $\gamma = 23.5$.

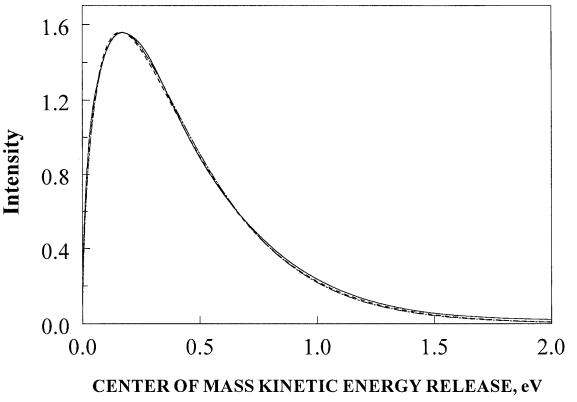

Fig. 1. Center-of-mass kinetic energy release distributions for the reaction $C_{60}^+ \rightarrow C_{58}^+ + C_2$; solid line: the experimental KERD; dashed line: the KERD obtained using the model free approach; dot-dash line: the KERD obtained from the SSP model (see text).

The experimental KERD and the ones calculated using the model free approach and the SSP model are shown in Fig. 1 and the results are summarized in Table 1. There is good agreement between the experimental KERD (solid line) and the models (dashed lines). Both models nearly overlap so that it is hard to distinguish between them. As mentioned earlier, the two models yield different C_2 binding energies. The difference in the binding energy obtained using the model free approach and the SSP model with the

Table 1
Model parameters for reaction $C_{60}^+ \rightarrow C_{58}^+ + C_2$ obtained using different models as described in the text

Parameter	Spherically symmetric potential		Model free approach
	Eq. (6)	Eq. (7)	
l			0.55 ± 0.01
$T^{\ddagger}$, K	2680	3190	3300
T_b, K	2870	3420	3540
ΔE_a, eV	6.0 ± 0.2	6.9 ± 0.2	7.2 ± 0.2

interaction potential given by Eq. (6) (see Table 1) is quite large (1.2 eV). However, when the more realistic interaction potential is assumed [Eq. (7), used in Fig. 1], the C_2 binding energy obtained from the SSP model gets much closer to the one obtained using the model free approach. We have found that Gorin's term plays an important role in the interaction between C_{58}^+ and C_2 due to a high polarizability of the fullerene cage. In the following calculations we will use both the model free approach and the SSP model with the potential given by Eq. (7).

4. Experimental results

4.1. The mixture of Tb containing fullerenes

Fig. 2 (a) and (b) represents the mass spectrum of a Tb containing fullerene mixture. The ion $Tb@C_{82}^+$ together with empty fullerenes up to C_{104}^+ and dimetallofullerenes from $Tb_2@C_{80}^+$ and up to $Tb_2@C_{96}^+$ are observed in the mass spectrum. Fig. 3 shows relative abundances of all the species $Tb_m@C_n^+$ ($m = 0, 1, 2$) observed in the mass spectrum normalized to the $Tb_m@C_{82}^+$ signal intensity. The mass distribution of fullerenes with two Tb atoms closely resembles the distribution of empty fullerenes present in the mixture with C_{84}^+ and $Tb_2@C_{84}^+$ being the most abundant species. On the other hand, the mass distribution of fullerenes with one Tb atom is very different. $Tb@C_{82}^+$ is the most abundant species, because of the presence of a small amount of the corresponding neutral in the fullerene mixture that is being ionized. Other ionized monometallofullerenes that are present

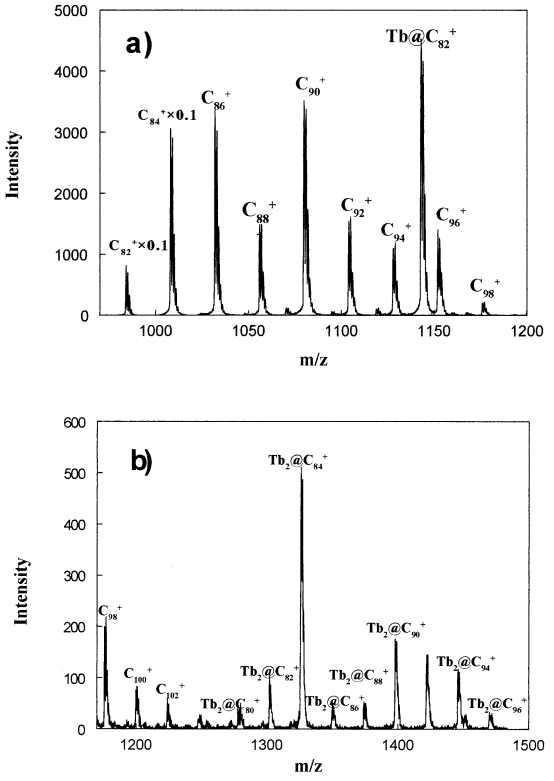

Fig. 2. The mass spectrum of a Tb containing fullerene mixture; (a) m/z range 900–1200 Thomson; (b) m/z range 1200–1500 Thomson.

only in trace amounts in the spectrum are probably formed from $Tb@C_{82}^+$ rather than by direct ionization of the corresponding neutrals. Fragment ions are usually of very low abundance in fullerene mass spectra, under the experimental conditions used in these studies.

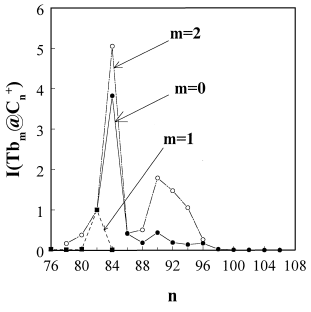

Fig. 3. Relative abundance of $Tb_m@C_n^+$ species ($m = 0, 1, 2$) normalized to the signal intensity of the corresponding $Tb_m@C_{82}^+$.

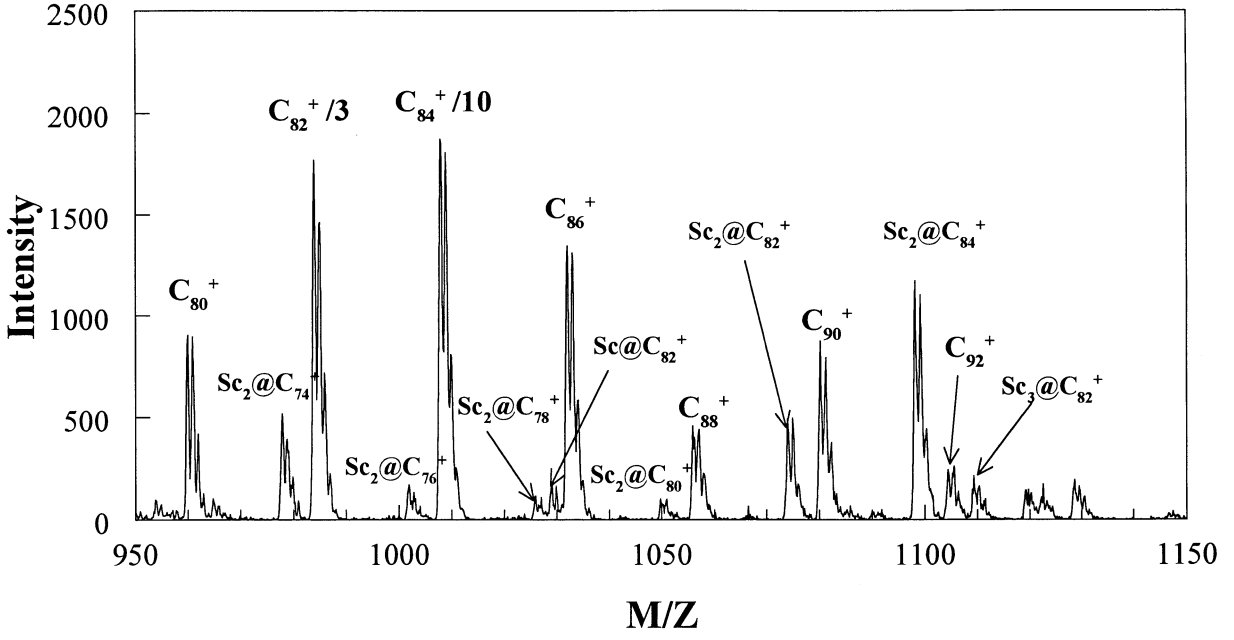

Fig. 4. The mass spectrum of a Sc containing fullerene mixture.

The similarity of the mass distributions obtained for empty fullerenes and fullerenes containing two Tb atoms may be understood if two endohedral atoms are trapped in the most stable fullerene cages. Theoretical calculations [37] suggested that two Sc atoms are equivalently encapsulated inside the most stable D_{2d} isomer of C_{84} along the C_2 axis. Later ^{13}C-NMR studies of $Sc_2@C_{84}$ have verified [38] that two Sc atoms are trapped mainly in the D_{2d} isomer of C_{84}. Nagase and co-workers have suggested [9] that metal atoms that transfer two valence electrons to the fullerene cage are likely to be stabilized in the D_{2d} isomer of C_{84}, whereas endohedral atoms that transfer three electrons are highly stabilized in the I_h cage of C_{80}. There are no theoretical predictions concerning Tb as an endohedral atom. Our observation of $Tb_2@C_{84}^+$ as the most abundant species among the ones with two metal atoms inside the cage suggests that Tb transfers two electrons to the fullerene cage like Sc does.

4.2. The mixture of Sc containing fullerenes

The mass spectrum of the Sc containing mixture is shown in Fig. 4. Empty fullerenes, $Sc@C_{72}^+$ and $Sc@C_{82}^+$, dimetallofullerenes $Sc_2@C_n^+$ (n = 58–88) and $Sc_3@C_{82}^+$ were found in the mass spectrum. Relative abundances of $Sc_m@C_n^+$ normalized to the $Sc_m@C_{82}^+$ signal intensity are shown in Fig. 5. $Sc_2@C_{84}^+$ is the most abundant species among the ones with two metal atoms inside the cage. However, the mass distribution obtained for the mixture of Sc containing fullerenes is quite different from the one for Tb containing species. The $Sc@C_{82}^+$ signal is only about 30% of the signal of $Sc_2@C_{82}^+$, whereas the $Tb@C_{82}^+$ signal was 50 times higher than that of $Tb_2@C_{82}^+$.

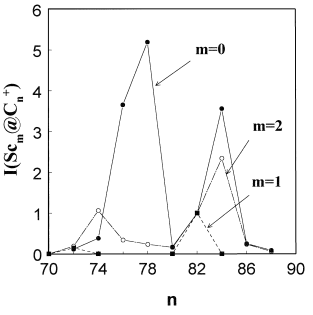

Fig. 5. Relative abundance of $Sc_m@C_n^+$ species (m = 0, 1, 2) normalized to the signal intensity of the corresponding $Sc_m@C_{82}^+$.

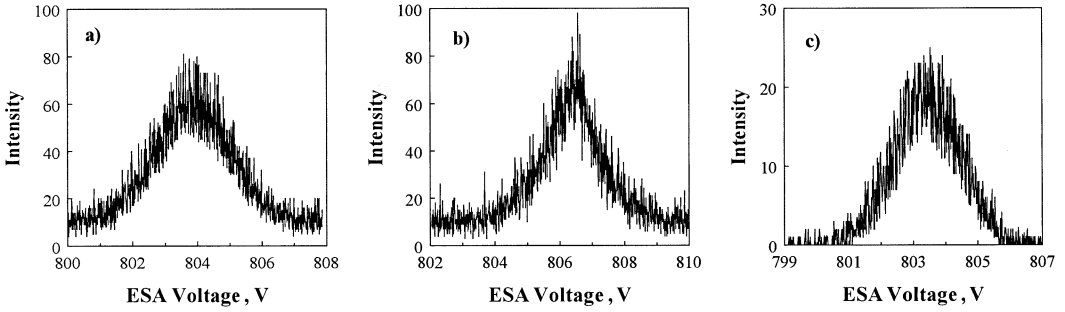

Fig. 6. Metastable peak shapes (a) for reaction (r1), (b) for reaction (r2), (c) for reaction (r3).

4.3. Fragmentation of metallofullerenes

Electric sector scans for preselected $Tb@C_{82}^+$, $Tb_2@C_{84}^+$, and $Sc_2@C_{84}^+$ over wide voltage ranges have shown the presence of metastable peaks due to the loss of C_2 units. No evidence for the release of endohedral atoms was found and no other fragmentation channels were observed.

Metastable peak shapes were determined for the following reactions:

$$Tb@C_{82}^+ \rightarrow Tb@C_{80}^+ + C_2 \quad \text{(r1)}$$

$$Tb_2@C_{84}^+ \rightarrow Tb_2@C_{82}^+ + C_2 \quad \text{(r2)}$$

$$Sc_2@C_{84}^+ \rightarrow Sc_2@C_{82}^+ + C_2 \quad \text{(r3)}$$

$$C_{84}^+ \rightarrow C_{82}^+ + C_2 \quad \text{(r4)}$$

The signal intensity for $Sc@C_{82}^+$ was too low to study its fragmentation. It should be mentioned here that the reactions

$$La@C_{82}^+ \rightarrow La@C_{80}^+ + C_2 \quad \text{(r5)}$$

$$C_{82}^+ \rightarrow C_{80}^+ + C_2 \quad \text{(r6)}$$

have been studied by us recently [12]. Metastable peak shapes obtained for reactions (r1)–(r3) are represented in Fig. 6. It has been demonstrated that metastable peaks that are due to reactions taking place in the second field free region (2FFR) of a double focusing mass spectrometer of reverse geometry suffer from artifacts because of decompositions in the first field free region (1FFR) of the instrument [39,40]. Decompositions of higher fullerenes in the 1FFR may interfere with fullerene ion decompositions in the 2FFR. For example, the artifact for the reaction $M@C_n^+ \rightarrow M@C_{n-2}^+ + C_2$ in the 2FFR may be due to the reaction $M@C_{n+4}^+ \rightarrow M@C_{n+2}^+ + C_2$ in the 1FFR. Therefore, the metastable peak for reaction (r1) may be disturbed by the fragmentation of $Tb@C_{86}^+$, for (r2) by $Tb_2@C_{88}^+$, for (r3) by $Sc_2@C_{88}^+$, and for (r4) by C_{88}^+. However, $Tb@C_{86}^+$ was not found in the Tb containing mixture, the amount of $Sc_2@C_{88}^+$ was on the background level and nearly no C_{88}^+ was present in the Sc containing mixture. Therefore, the metastable peaks for reactions (r1), (r3), and (r4) do not contain artifacts. On the other hand, the metastable peak for reaction (r2) contains an artifact and one has to subtract it in order to get the correct kinetic energy release for reaction (r2). The artifact peak could not be resolved from the main peak under our experimental conditions and therefore the subtraction procedure became difficult. We have found that an accurate KERD could not be derived from the metastable peak for reaction (r2). We will report only the value for the average KER for this reaction.

Average KERs are summarized in Table 2. The larger error bar obtained for $Tb_2@C_{84}^+$ is due to the presence of the experimental artifacts as discussed above. Two interesting observations should be pointed out: (1) The average KER for $Tb@C_{82}^+$ is greater than the average KER for $La@C_{82}^+$ obtained previously, i.e. a Tb atom stabilizes the C_{82} cage even more than a La atom; (2) two Sc atoms have a slight destabilizing effect on the C_{84} cage, whereas two Tb atoms strongly stabilize it.

Table 2
Average KERs for reactions (r1)–(r6)

	C_{82}^+	La@C_{82}^+	Tb@C_{82}^+	C_{84}^+	Tb_2@C_{84}^+	Sc_2@C_{84}^+
⟨KER⟩, eV	0.35 ± 0.02*	0.46 ± 0.02*	0.55 ± 0.02	0.45 ± 0.02	0.57 ± 0.04	0.42 ± 0.02

*[12]

Center-of-mass product KERDs for reactions (r1), (r3) and (r4) have been derived from the corresponding metastable peak shapes. All the distributions have been modeled using the SSP model and the model free approach. Table 3 summarizes the parameters used for the SSP calculations. Molecular polarizabilities of fullerenes have been estimated using the known polarizabilities of single and double C–C bonds [41]. The mean polarizability of a single C–C bond is 0.64×10^{-24} cm^3 and of a double bond is 1.66×10^{-24} cm^3. (The same method has been used by Guha et al. [42] with slightly different values of 0.672×10^{-24} cm^3 for the single C–C bond and 1.63×10^{-24} cm^3 for the double bond). For example, there are 60 single and 30 double bonds in C_{60} so that the molecular polarizability is 88.2×10^{-24} cm^3 which is in good agreement with the experimental and theoretically predicted values [35]. The molecular polarizability of C_{60} calculated in this way is about 4% higher than the experimental value of 84×10^{-24} cm^3 and the polarizability of C_{70} is 9% higher than the experimentally measured one of 94×10^{-24} cm^3 [43,44]. The polarizabilities of C_{80} and C_{82} calculated on this basis (see Table 3) may be overestimated by about 15%. However, the effect of this overestimation on the binding energy is very small so that these values are accurate enough for our purposes. The results of the modeling are summarized in Table 4.

4.4. Endohedral fullerenes with noble gases

The only metastable peak for Ar@C_{60}^+ and Kr@C_{60}^+ observed in the MIKE spectrum is due to the C_2 loss reaction. No evidence for the unimolecular release of an endohedral atom was found. Metastable peak shapes for reactions

$$\text{Ar@}C_{60}^+ \rightarrow \text{Ar@}C_{58}^+ + C_2 \quad \text{(r7)}$$

$$\text{Kr@}C_{60}^+ \rightarrow \text{Kr@}C_{58}^+ + C_2 \quad \text{(r8)}$$

Table 3
Parameters for the SSP model calculations for M@C_n^+

	C_{82}^+	La@C_{82}^+	Tb@C_{82}^+	C_{84}^+	Sc_2@C_{84}^+
Moment of inertia of ionic fragment (g cm^2/10^{-36})[a]	1.824	1.887	1.900	1.885	1.946
Impact parameter between product fragments (cm)[b]	4.727×10^{-8}	4.727×10^{-8}	4.727×10^{-8}	4.776×10^{-8}	4.776×10^{-8}
Polarizability of ionic fragment (cm^3/10^{-24})[c]	120	120	120	123	123
Ionization energy of M@C_{n-2}	6.6[d]	6.19[e]	6.19[f]	6.56[g]	6.56[h]

[a]The molecules were treated as elliptic shells with moment of inertia $I = \frac{1}{3} m(r_1^2 + r_2^2)$. The geometry of C_{80} was adopted from [45], the geometry of C_{82} from [46].
[b]$b = r_{av} + r_{C-C}/2$, where r_{av} is the average radius of fullerene cage, $r_{C-C} = 1.243$ is the C–C bond length in C_2.
[c]Estimated using the bond polarizabilities as discussed in the text.
[d]Estimated.
[e]Assumed to be the same as the ionization energy of La@C_{82} from [47].
[f]Assumed to be the same as for La@C_{82}.
[g][48]
[h]Assumed to be the same as for C_{84}.

Table 4
Modeling results for metallofullerenes

	Model free approach				SSP model		
	l	$T^{\ddagger}$, K	T_b, K	ΔE_{vap}, eV	$T^{\ddagger}$, K	T_b, K	ΔE_{vap}, eV
C_{82}^+	0.51 ± 0.01	2860 ± 20	3010 ± 30	6.1 ± 0.4	2490 ± 20	2620 ± 30	5.3 ± 0.4
$La@C_{82}^+$	0.60 ± 0.01	3620 ± 20	3800 ± 30	7.7 ± 0.5	3190 ± 20	3350 ± 30	6.9 ± 0.5
$Tb@C_{82}^+$	0.52 ± 0.02	4650 ± 20	4880 ± 30	9.2 ± 0.5	3540 ± 20	3720 ± 30	8.0 ± 0.5
C_{84}^+	0.55 ± 0.01	3540 ± 20	3710 ± 30	7.5 ± 0.4	3000 ± 20	3150 ± 30	6.6 ± 0.4
$Sc_2@C_{84}^+$	0.50 ± 0.01	3430 ± 20	3600 ± 30	7.3 ± 0.4	2960 ± 20	3100 ± 30	6.5 ± 0.4

are shown in Fig. 7. The fragmentation of $Kr@C_{60}^+$ was studied under relatively high pressure in the 2FFR ($\approx 1 \times 10^{-7}$ Torr). The left part of the metastable peak for reaction (r8) contains, therefore, the contribution of a collision-induced dissociation.

The center-of-mass product KERDs were derived from the metastable peaks and modeled as described before. The results of the modeling are summarized in Table 5.

5. Discussion

Tables 4 and 5 and Fig. 8 (a) and (b) summarize the binding energies obtained from the modeling of the KERDs; Fig. 9 shows the comparison between the experimental KERDs for the C_2 loss reaction for C_{60}^+ and the noble gas complexes. Binding energies of the noble gas containing endohedral fullerenes [Fig. 8 (a), Table 5] increase with the size of the endohedral atom. The SSP model yields systematically lower values. This is probably because of the slight inaccuracy in the interaction potential that was assumed. However, the differences between the values obtained from the SSP model and the model free approach are not large and the values are nearly the same within the experimental error. The fitting parameter l used in the model free approach is the same for all the noble gas containing fullerenes and for empty C_{60}^+ indicating that the interaction potential between the separating fragments is not influenced by the presence of the noble gas atom.

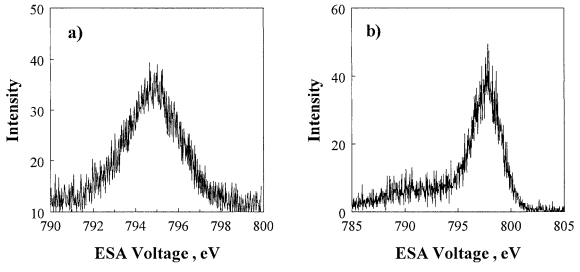

Fig. 7. Metastable peak shapes (a) for reaction (r7), (b) for reaction (r8).

There is serious disagreement between theoretical predictions concerning the relative stability of endohedral noble gas containing fullerenes. Pang and Brisse [49] have predicted from empirical Lennard-Jones potentials that only He, Ne, and Ar can form a stable complex with C_{60} whereas Kr and Xe cannot form stable endohedral complexes with C_{60} due to their large Van der Waals radii. Son and Sung [50]

Table 5
Modeling results for noble gas containing fullerenes

	Model free approach				SSP model		
	l	$T^{\ddagger}$, K	T_b, K	ΔE_{vap}, eV	$T^{\ddagger}$, K	T_b, K	ΔE_{vap}, eV
C_{60}^+	0.55 ± 0.01	3300 ± 20	3540 ± 30	7.2 ± 0.2	3190 ± 20	3420 ± 30	6.9 ± 0.2
$Ne@C_{60}^+$	0.55 ± 0.01	3510 ± 20	3770 ± 30	7.6 ± 0.4	3470 ± 20	3720 ± 30	7.5 ± 0.4
$Ar@C_{60}^+$	0.55 ± 0.01	3760 ± 20	4030 ± 30	8.2 ± 0.4	3570 ± 20	3830 ± 30	7.8 ± 0.4
$Kr@C_{60}^+$	0.55 ± 0.01	4120 ± 20	4410 ± 30	8.9 ± 0.5	3920 ± 20	4200 ± 30	8.5 ± 0.5

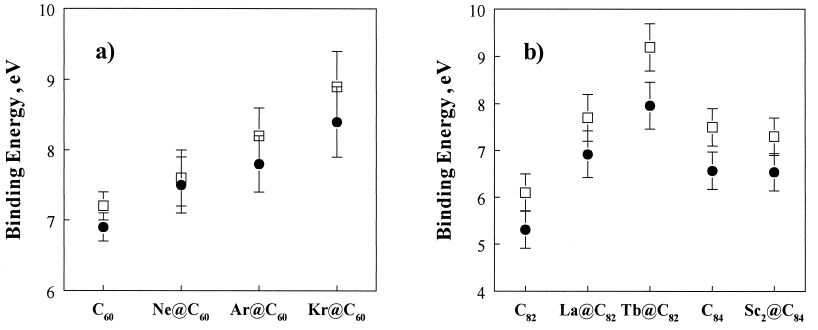

Fig. 8. C_2 binding energies, (a) for noble gas containing fullerenes, (b) for metallofullerenes, obtained using the model free approach (open square) and the SSP model (filled circle) as described in the text.

have used the same empirical approach to deduce that the stability of the endohedral noble gas containing fullerenes increases in the order Xe < He < Ne < Kr < Ar with Ar@C_{60} being the most stable complex. Jiménez-Vázquez and Cross [51] have calculated binding energies from the potentials of Pang and Brisse [49] and demonstrated that all five noble gases bind with C_{60}. Ab initio Hartree–Fock calculations account for the Pauli repulsions between the noble gas atoms and the C_{60} cage, but not for the attractive dispersion forces. Consequently, they predict a destabilization of these endohedral complexes [52] which increases with increasing size of the noble gas [53]. Patchkovskii and Thiel [54] have shown in an extensive study of He@C_{60} that the dispersion can be included at the ab initio MP2 level (Møeller-Plesset second-order perturbation theory). In subsequent MP2 calculations, Thiel and co-workers [55] find that all the noble gas atoms stabilize C_{60} with the stability increasing in the order He < Ne < Ar < Xe < Kr. Contradictory MP2 results have been published by Darzynkiewicz and Scuseria [53] which, however, have been corrected in an erratum: the original "MP2" data were actually Hartree–Fock data, and the revised MP2 results from the erratum are consistent with those published earlier [55]. Hence, this question seems to have been finally settled.

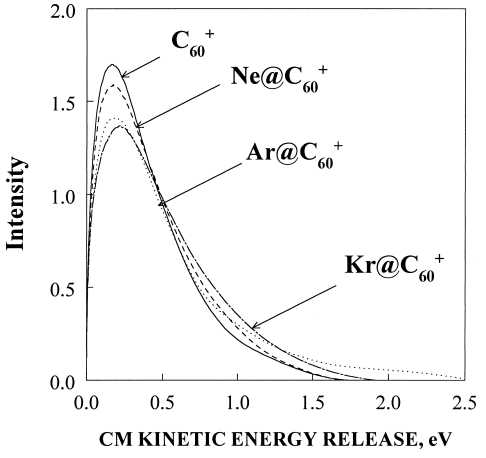

Fig. 9. Experimental center-of-mass KERDs. Solid line: reaction $C_{60}^+ \rightarrow C_{58}^+ + C_2$; dashed line: reaction $Ne@C_{60}^+ \rightarrow Ne@C_{58}^+ + C_2$; dotted line: reaction (r7); dot-dash line: reaction (r8).

Our present experimental results are for C_2 evaporations from ionized noble gas endohedral fullerenes. It may be assumed that the stability order deduced for the neutral species remains valid also for the ions. Furthermore, the noble gas atom binding energies in the ions are probably higher than in the respective neutrals, because of contributions from ion-induced dipole interactions. Reactions (r7) and (r8) can be included in a thermochemical cycle as follows:

$$\begin{array}{ccc} & \xrightarrow{\Delta E_1} & \\ Ar@C_{60}^+ & \rightarrow & Ar@C_{58}^+ + C_2 \\ \Delta E_3 \downarrow & & \downarrow \Delta E_2 \\ Kr@C_{60}^+ & \rightarrow & Kr@C_{58}^+ + C_2 \\ & \xrightarrow{\Delta E_4} & \end{array}$$

Scheme 1

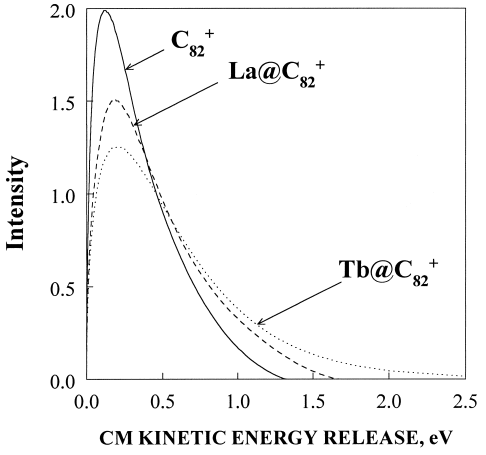

Fig. 10. Experimental center-of-mass KERDs. Solid line: reaction (r6); dashed line: reaction (r5); dotted line: reaction (r1).

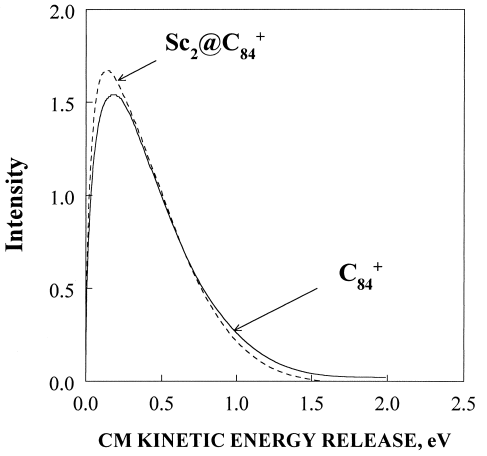

Fig. 11. Experimental center-of-mass KERDs. Solid line: reaction $C_{84}^+ \rightarrow C_{82}^+ + C_2$; dashed line: reaction (r3).

We have found that $\Delta E_1 < \Delta E_4$. Since $\Delta E_1 + \Delta E_2 = \Delta E_3 + \Delta E_4$, therefore $\Delta E_2 > \Delta E_3$. Thus Kr could have a larger binding energy in C_{60}^+ than Ar but be less likely to lose C_2 because the binding energy of Kr in C_{58}^+ is less.

The C_2 binding energies of metallofullerenes are presented in Fig. 8 (b) and Table 4. The agreement between the SSP model and the model free approach is worse than it was for noble gas endohedral fullerenes, however both models show the same trend. It should be mentioned here that we did not account for the polarizability brought about by the metal atom. The comparison between the KERDs for reactions (r1), (r5), and (r6) is shown in Fig. 10 and for reactions (r3) and (r4) in Fig. 11. Endohedral metal atoms have a strong stabilizing effect on the C_{82} cage. The terbium atom has a much stronger effect that the lanthanum atom (the C_2 binding energy for $Tb@C_{82}^+$ is at least 1 eV higher than that for $La@C_{82}^+$). $Sc_2@C_{84}^+$ has a slightly lower C_2 binding energy than does C_{84}^+. The binding energy for $Tb_2@C_{84}^+$ could not be derived from the metastable peak due to the artifacts as discussed earlier. However, the average kinetic energy release for the C_2 loss reaction from $Tb_2@C_{84}^+$ is larger than for C_{84}^+ and for $Sc_2@C_{84}^+$ implying that two terbium atoms stabilize the C_{84} cage. Each terbium atom seems to donate two valence electrons to the cage. If the properties of metallofullerenes were determined only by the number of electrons that the endohedral atom transfers to the cage it occupies, then one would expect to find a similar behavior of Tb and Sc containing species. However, their behavior is quite different as manifested by their influence on the C_{84}^+ cage and by the different mass distributions observed in their mass spectra (Figs. 3 and 5). For example, the intensity ratio of $Tb@C_{82}^+$ and $Tb_2@C_{82}^+$ is 50:1, whereas the intensity ratio of $Sc@C_{82}^+$ and $Sc_2@C_{82}^+$ is 1:3. The electronic structure of Sc and Tb is very different. Terbium has a partly filled f-shell which could be responsible for the different behavior of the terbium atoms as compared to the scandium atoms. Further study of the unimolecular fragmentation of metallofullerenes is needed to better understand the influence of the endohedral atom on the energetics of the breaking of the cage.

It should be pointed out that a Gspann parameter $\gamma = 23.5$ was employed in our modeling. The Gspann parameter is defined as $\gamma = \ln A - \ln k_{mp}$, where A is the preexponential factor for the reaction and k_{mp} is the most probable rate constant sampled in the experiment. The value of 23.5 was obtained [56] assuming $A = 1.6 \times 10^{15}$ s^{-1} and a most probable rate constant of $k_{mp} = 1 \times 10^5$ s^{-1}. A somewhat higher value $\gamma = 25.6$ has been obtained by Wörgötter et al. [17] for C_{60}^+ from the modeling of experimental

appearance energies of fullerenes. An even higher Gspann parameter ($\gamma = 31$) was found by Hansen and Campbell [57] from the analysis of metastable fractions of fullerenes. Fullerenes undergo efficient cooling which is due to emission in the visible and ultraviolet [57–59], therefore the most probable dissociative rate constant sampled in the experiment is defined not only by the flight time of the fullerene ion in the mass spectrometer but also by the rate of radiative cooling. The value of 1×10^5 s^{-1} is the upper bound for the most probable rate constant and the Gspann parameter should be higher than 23.5. Higher binding energies are obtained if a higher Gspann parameter is employed. For example, the C_2 binding energy for C_{60}^+ obtained from the model free approach with $\gamma = 31$ is $\Delta E(C_{60}^+) = 9.7$ eV. The binding energies of endohedral fullerenes will rise correspondingly. Unfortunately, the preexponential factor for the C_2 loss reaction is still unknown and the extent to which the radiative cooling slows down the most probable rate constant is hard to estimate. Therefore, the true value for the Gspann parameter is not well-defined. However, although the absolute C_2 binding energies may be about 30% higher than the ones based on $\gamma = 23.5$, the relative values deduced in this work are considered to be correct.

Note added in proof:

We have recently obtained new evidence in favor of a high C_2 binding energy in C_{60} and in C_{60}^+ on the basis of time resolved measurements of metastable fractions [60]. The measurements were modeled independently of any prior knowledge of the preexponential A factor or Gspann parameter. The results obtained were $A = 2 \times 10^{19}$ s^{-1} and $\Delta E(C_{60}^+) = 9.5$ eV[5]. The Gspann parameter corresponding to the A factor [60] is $\gamma = 33$ provided $k_{mp} = 10^5$ s^{-1}. All the binding energies for the endohedral ions studied here should be raised accordingly by a factor of 9.5/7.2 = 1.3, i.e. by 30%, as noted earlier.

Acknowledgements

The research was supported by grant no. 94-00058 from the United States-Israel Binational Science Foundation (BSF), Jerusalem, Israel. The Farkas Center is supported by the Minerva Gesellschaft für die Forschung GmbH, München.

References

[1] (a) J.R. Heath, S.C. O'Brien, Q. Zhang, Y. Liu, R.F. Curl, H.W. Kroto, F.K. Tittel, R.E. Smalley, J. Am. Chem. Soc. 107 (1985) 7779. (b) H.W. Kroto, J.R. Heath, S.C. O'Brien, R.F. Curl, R.E. Smalley, Nature 318 (1985) 162.
[2] (a) Y. Chai, T. Guo, C. Jin, R.E. Haufler, L.P.F. Chibante, J. Fure, L. Wang, J.M. Alford, R.E. Smalley, J. Phys. Chem. 95 (1991) 7564. (b) R.D. Johnson, M.S. de Vries, J.R. Salem, D.S. Bethune, C.S. Yanoni, Nature 355 (1992) 239.
[3] C.-H. Park, B.O. Wells, J. DiCarlo, Z.-X. Shen, J.R. Salem, D.S. Bethune, C.S. Yannoni, R.D. Johnson, M.S. de Vries, C. Booth, F. Bridges, P. Pianetta, Chem. Phys. Lett. 213 (1993) 196.
[4] K.B. Shemilov, D.E. Clemmer, M.F. Jarrold, J. Phys. Chem. 99 (1995) 11376.
[5] M. Takata, B. Umeda, E. Nishibori, M. Sakata, Y. Saito, M. Ohno, H. Shinohara, Nature 377 (1995) 46.
[6] S. Nagase, K. Kobayashi, T. Akasaka, J. Comput. Chem. 19 (1998) 232.
[7] L. Moro, R.S. Ruoff, C.H. Becker, D.C. Lorents, R. Malhotra, J. Phys. Chem. 97 (1993) 6801.
[8] S. Nagase, K. Kobayashi, T. Akasaka, Bull. Chem. Soc. Jpn. 69 (1996) 2131 and references therein.
[9] S. Nagase, K. Kobayashi, T. Akasaka, J. Mol. Struct. (Theochem) 398 (1997) 221.
[10] D.C. Lorents, D.H. Yu, C. Brink, N. Jensen, P. Hvelplund, Chem. Phys. Lett. 236 (1995) 141.
[11] S. Suzuki, Y. Kojima, Y. Achiba, T. Wakabayashi, R. Tellgmann, E.E.B. Campbell, I.V. Hertel, Z. Phys. D. 40 (1997) 410.
[12] J. Laskin, H.A. Jiménez-Vázquez, R. Shimshi, M. Saunders, M.S. de Vries, C. Lifshitz, Chem. Phys. Lett. 242 (1995) 249.
[13] T. Weiske, D.K. Böhme, J. Hrusák, W. Krätschmer, H. Schwarz, Angew. Chem. Intern. Ed. 30 (1991) 884.
[14] T. Weiske, J. Hrusák, D.K. Böhme, H. Schwarz, Helv. Chim. Acta 1992, 75 (1992) 79.
[15] M. Saunders, H.A. Jiménez-Vázquez, R.J. Cross, R.J. Poreda, Science 259 (1993) 1428.
[16] M. Saunders, H.A. Jiménez-Vázquez, R.J. Cross, S. Mroczkowski, M.L. Gross, D.E. Giblin, R.J. Poreda, J. Am. Chem. Soc. 116 (1994) 2193.
[17] R. Wörgötter, B. Dünser, P. Scheier, T.D. Märk, M. Foltin, C.E. Klots, J. Laskin, C. Lifshitz, J. Chem. Phys. 104 (1996) 1225.
[18] (a) E.E.B. Campbell, R. Ehlich, A. Hielscher, J.M.A. Frazao,

I.V. Hertel, Z. Phys. D 23 (1992) 1. (b) R. Kleiser, H. Sprang, S. Furrer, E.E.B. Campbell, Z. Phys. D 28 (1993) 89.
[19] (a) S. Patchkovskii, W. Thiel, Helv. Chim. Acta 80 (1997) 495. (b) R. Shimshi, A. Khong, H.A. Jiménez-Vázquez, R.J. Cross, M. Saunders, Tetrahedron 52 (1996) 5143.
[20] B.A. DiCamillo, R.L. Hettich, G. Guiochon, R.N. Compton, M. Saunders, H.A. Jiménez-Vázquez, A. Khong, R.J. Cross, J. Phys. Chem. 100 (1996) 9197.
[21] C. Brink, P. Hvelplund, H. Shen, H.A. Jiménez-Vázquez, R.J. Cross, M. Saunders, Chem. Phys. Lett., unpublished.
[22] D. Giblin, M.L. Gross, M. Saunders, H.A. Jiménez-Vázquez, R.J. Cross, J. Am. Chem. Soc. 119 (1997) 9883.
[23] (a) P.P. Radi, M.E. Rincon, M.T. Hsu, J. Brodbelt-Lustig, P. Kemper, M.T. Bowers, J. Phys. Chem. 93 (1989) 6187. (b) P.P. Radi, M.-T. Hsu, M.E. Rincon, P.R. Kemper, M.T. Bowers, Chem. Phys. Lett. 174 (1990) 223. (c) P.A.M. van Koppen, J. Brodbelt-Lustig, M.T. Bowers, J. Am. Chem. Soc. 112 (1990) 5663. (d) P.A.M. van Koppen, J. Brodbelt-Lustig, M.T. Bowers, J. Am. Chem. Soc. 113 (1991) 2359.
[24] P.P. Morgan, J.H. Beynon, R.H. Bateman, B.N. Green, Intern. J. Mass Spectrom. Ion Phys. 28 (1978) 171.
[25] N.J. Kirshner, M.T. Bowers, J. Phys. Chem. 91 (1987) 2573.
[26] C. Lifshitz, F. Louage, J. Phys. Chem. 93 (1989) 6533.
[27] J.L. Holmes, A.D. Osborne, Intern. J. Mass Spectrom. Ion Phys. 23 (1977) 189.
[28] C. Lifshitz, E. Tzidony, Intern. J. Mass Spectrom. Ion Phys. 39 (1981) 181.
[29] M.F. Jarrold, W. Wagner-Redeker, A.J. Allies, N.J. Kirchner, M.T. Bowers, Intern. J. Mass Spectrom. Ion Processes 58 (1984) 63.
[30] (a) C.E. Klotz, Z. Phys. D 21 (1991) 335. (b) P. Sandler, T. Peres, G. Weissman, C. Lifshitz, Ber. Bunsenges. Phys. Chem. 96 (1992) 1195.
[31] (a) P. Sandler, C. Lifshitz, C.E. Klots, Chem. Phys. Lett. 200 (1992) 445. (b) C.E. Klots, J. Chem. Phys. 98 (1993) 1110.
[32] (a) R.D. Levine, R.B. Bernstein, Molecular Reaction Dynamics and Chemical Reactivity, Oxford University, New York, 1987, pp. 274–275. (b) T. Baer, W.L. Hase, Unimolecular Reaction Dynamics, Oxford University, New York, 1996, pp. 173–174. (c) P. Urbain, F. Remacle, B. Leyh, J.C. Lorquet, J. Phys. Chem. 100 (1996) 8003.
[33] C. Lifshitz, in T. Baer, C.Y. Ng, I. Powis, (Eds.), The Wiley Series in Ion Chemistry and Physics: Cluster Ions, Wiley, New York, 1993, Chap. 2, pp. 121–164.
[34] C.E. Klots, J. Chem. Phys. 100 (1994) 1035.
[35] A.A. Quong, M.R. Pederson, Phys. Rev. B 46 (1992) 12906.
[36] J.A. Zimmerman, J.R. Eyler, S.B.H. Back, S.W. McElvany, J. Chem. Phys. 94 (1991) 3556.
[37] S. Nagase, K. Kobayashi, Chem. Phys. Lett. 231 (1994) 319.
[38] E. Yamamoto, M. Tansho, T. Tomiyama, H. Shinohara, H. Kawahara, Y. Kobayashi, J. Am. Chem. Soc. 118 (1996) 2293.
[39] T. Drewello, K.-D. Asmus, J. Stach, R. Herzschuh, M. Kao, C.S. Foote, J. Phys. Chem. 95 (1991) 10554.
[40] C. Lifshitz, J. Laskin, T. Peres, Org. Mass Spectrom. 28 (1993) 1001.
[41] J.O. Hirschfelder, C.F. Curtiss, R.B. Bird, Molecular Theory of Gases and Liquids, Wiley, New York, 1954, pp. 941–957.
[42] S. Guha, J. Menédez, J.B. Page, G.B. Adams, Phys. Rev. B, 53 (1996) 13106.
[43] B. Shanker, J. Applequist, J. Phys. Chem. 98 (1994) 6846.
[44] S.-L. Ren, K.-A. Wang, P. Zhou, Y. Wang, A.M. Rao, M.S. Meier, J.P. Selegue, P.C. Eklund, Appl. Phys. Lett. 61 (1992) 124.
[45] K. Nakao, N. Kurita, M. Fujita, Phys. Rev. B 94 (1994) 11415.
[46] S. Nagase, K. Kobayashi, T. Kato, Y. Achiba, Chem. Phys. Lett. 201 (1993) 475.
[47] S. Nagase, K. Kobayashi, Chem. Phys. Lett. 228 (1994) 106.
[48] J. Cioslowski, K. Raghavachari, J. Chem. Phys. 98 (1993) 8734.
[49] L. Pang, F. Brisse, J. Phys. Chem. 97 (1993) 8562.
[50] M.-S. Son, Y.K. Sung, Chem. Phys. Lett. 245 (1995) 113.
[51] H.A. Jiménez-Vázquez, R.J. Cross, J. Chem. Phys. 104 (1996) 5589.
[52] J. Cioslowski, E.D. Fleischmann, J. Chem. Phys. 94 (1991) 3730.
[53] R.B. Darzynkiewicz, G.E. Scuseria, J. Phys. Chem. 101 (1997) 7141; Erratum, in press.
[54] S. Patchkovskii, W. Thiel, J. Chem. Phys. 106 (1997) 1796.
[55] M. Bühl, S. Patchkovskii, W. Thiel, Chem. Phys. Lett. 275 (1997) 14.
[56] C.E. Klots, Int. J. Mass Spectrom. Ion Processes 100 (1990) 457.
[57] K. Hansen, E.E.B. Campbell, J. Chem. Phys. 104 (1996) 5012.
[58] E. Kolodney, A. Budrevich, B. Tsipinyuk, Phys. Rev. Lett. 74 (1995) 510.
[59] J. Laskin, C. Lifshitz, Chem. Phys. Lett. 277 (1997) 564.
[60] J. Laskin, B. Hadas, T.D. Märk, C. Lifshitz, Int. J. Mass Spectrom. 177 (1998) L9.